An experimental evaluation of Helmholtz potentials as a source of acoustic emission due to fatigue crack

Mohammad Faisal Haider*[a], Roshan Joseph[a], Victor Giurgiutiu[a]
[a]Department of Mechanical Engineering, University of South Carolina,
300 Main Street, Columbia, SC 29208

ABSTRACT

A novel method is proposed in this paper to extract acoustic emission (AE) source using Helmholtz potentials approach. In order to characterize the source in terms of potentials the underlying physics is to detect the AE signals and then develop an inverse algorithm to characterize the source. According to the new concept, the source can be characterized it provides the excitation potential information from the crack and that can be used to diagnose the crack (crack type and crack growth etc.). An AE experiment was designed to measure the acoustic emissions from the fatigue crack growth. A test specimen was made of 1 mm thick 304-steel material. A small hole (1 mm diameter) was drilled at the center of the specimen to initiate the fatigue crack. The specimen was subjected to the cyclic loadings by using the hydraulic MTS machine. AE waveforms are generated by convolutions of AE source functions, plate transfer functions. An inverse algorithm was developed to characterize the source of AE signal. AE signal analysis are done to determine AE source function using deconvolution process.

Keywords: Structural health monitoring, acoustic emission, guided wave propagation, Helmholtz potentials, inverse problem, deconvolution, AE source rise time, fatigue crack

1. INTRODUCTION

AE events in metallic or composite materials can be generated due to various phenomena like friction, plastic deformation, crack growth event etc. Of all the causes, crack growth event is a problem of great practical importance in metals due to the after effects it can cause towards the damage of the structure. A novel inverse algorithm for AE source characterization from AE signals detected during a fatigue crack growth event is discussed in this paper. Piezoelectric wafer active sensors (PWAS) were used for recording AE signals during a fatigue experiment and the signals were used for characterizing the AE source using the theoretical formulations.

AE signals may be generated by a wide range of phenomena such as micro-cracks, friction in existing cracks, dislocations, phase transformations, etc. The AE wave field generated by an AE event propagates in thin-wall structures such as plates in the form of guided waves. Many researchers studied AE due to various kinds of sources. Acoustic emission in thin plates during crack growth event was investigated in many researches [1], [2]. Acoustic emission due to rubbing in a rotor-bearing and source localization was studied by Wang et al. [3]. Acoustic emission in composite materials was also studied for progressive damage in a polymer-based composite [4]; clustering of AE signals obtained from failure in carbon fiber reinforced plastic (CFRP) specimens was also studied [5]. Acoustic emission during various fracture activities was studied to relate the fracture and AE signals [6]. McBride et al [7] investigated the relationship between acoustic emission amplitude and size of intermetallic inclusions at the fracture face. Barile et al [8] used the acoustic emission technique to monitor delamination in a unidirectional CFRP subjected to mode I loading. They concluded that it is possible to follow delamination effects in CFRP through proper monitoring of variation of the AE features. Various studies on acoustic energy harvesting was reported in the literatures [9]–[11].

Many researchers have done numerical and theoretical modeling and simulation of AE signals. Some of the studies performed numerical modeling of AE signals using Lamb waves [12], [13]. Finite element modeling and simulation of AE forward problem was performed [14]–[17]. Monopole or dipole definition of AE sources was used for modeling AE sources in several studies [12], [13], [18]. Definition of AE source by considering the AE source as a self-equilibrating seismic moment tensor was studied, and analytical formulations were developed for half-space and bulk medium in many pieces of research [19] [20]. In a recent study of AE guided wave propagation in a plate [21-23], the AE source was modeled as Helmholtz excitation potentials.

*Corresponding author email: haiderm@email.sc.edu

2. THEORY

When a crack grows in a solid material, a region of material adjacent to the free surfaces is unloaded, and its strain energy released. The strain energy release rate is the energy that must be supplied to a crack tip for it to grow and it must be balanced by the amount of energy dissipated due to the formation of new surfaces and other dissipative processes such as plasticity. The strain energy released from a crack can be correlated with the excitation potentials.

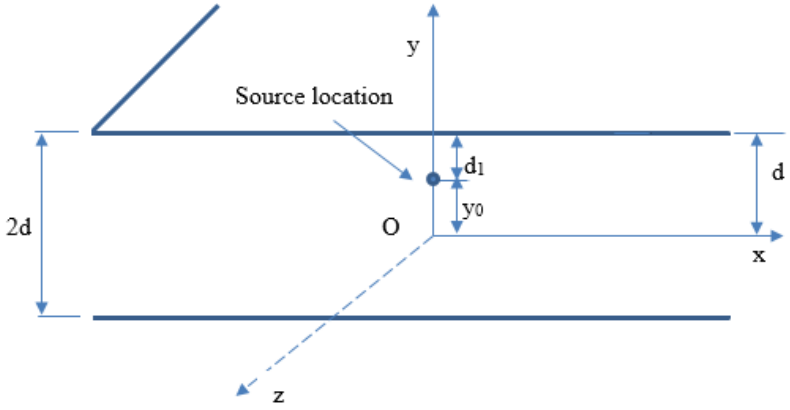

Figure 1. Plate of thickness 2d in which straight crested Lamb waves (P+SV) propagate in the x direction due to concentrated potentials.

Figure 1 shows the plate of thickness 2d in which straight crested Lamb waves (P+SV) propagate in the x direction due to concentrated potentials at d_1 distance from the top.

Navier-Lame equations in the absence of excitation force in vector form for Cartesian coordinates given as

$$(\lambda+\mu)\vec{\nabla}\left(\vec{\nabla}\cdot\vec{u}\right)+\mu\nabla^2\vec{u}=\rho\ddot{\vec{u}} \tag{1}$$

where, $\vec{u}=u_x\hat{i}+u_y\hat{j}+u_z\hat{k}$, with $\hat{i}$, $\hat{j}$, $\hat{k}$ being unit vectors in the x, y, z directions respectively. If the excitation force is present, then the Navier-Lame equation can be written as follow

$$(\lambda+\mu)\vec{\nabla}\left(\vec{\nabla}\cdot\vec{u}\right)+\mu\nabla^2\vec{u}+\rho\vec{f}=\rho\ddot{\vec{u}} \tag{2}$$

Assume that the displacement $\vec{u}$ can be expressed in terms of two potential functions, a scalar potential Φ and a vector potential $\vec{H}$, where

$$\vec{H}=H_x\vec{i}+H_y\vec{j}+H_z\vec{k} \tag{3}$$

$$\vec{u}=grad\ \Phi+curl\ \vec{H}=\vec{\nabla}\Phi+\vec{\nabla}\times\vec{H} \tag{4}$$

This equation is known as the Helmholtz equation, and is complemented by the uniqueness condition

$$\vec{\nabla}\cdot\vec{H}=0 \tag{5}$$

Introducing additional scalar and vector potentials A^* and $\vec{B}^*$ for body force $\vec{f}$

$$\vec{f}=grad\ \mathrm{A}^*+curl\ \vec{B}^*=\vec{\nabla}\mathrm{A}^*+\vec{\nabla}\times\vec{B}^* \tag{6}$$

Here,

$$\vec{B}^* = B_x^*\vec{i} + B_y^*\vec{j} + B_z^*\vec{k} \tag{7}$$

The uniqueness condition is,

$$\vec{\nabla}\cdot\vec{B}^* = 0 \tag{8}$$

Using the Equation (4) and (6), components of equation (2) can be written as,

$$\vec{\nabla}[(\lambda+2\mu)(\nabla^2\Phi) + \rho\mathrm{A}^* - \rho\ddot{\Phi}] + \vec{\nabla}\times(\mu\nabla^2\vec{H} + \rho\vec{B}^* - \rho\ddot{\vec{H}}) = \vec{0} \tag{9}$$

Upon rearrangement

$$c_P^2\nabla^2\Phi + \mathrm{A}^* = \ddot{\Phi} \tag{10}$$

$$c_S^2\nabla^2\vec{H} + \vec{B}^* = \ddot{\vec{H}} \tag{11}$$

were, $c_P^2 = \dfrac{\lambda+2\mu}{\rho}$; $c_S^2 = \dfrac{\mu}{\rho}$

For P+SV waves, the relevant potentials are $\Phi, H_z, \mathrm{A}, B_z$. Equations (10) and (11) condensed to two equations

$$c_P^2\nabla^2\Phi + A^* = \ddot{\Phi} \tag{12}$$

$$c_S^2\nabla^2 H_z + B_z^* = \ddot{H}_z \tag{13}$$

Upon rearranging

$$\nabla^2\Phi + \frac{1}{c_P^2}A^* = \frac{1}{c_P^2}\ddot{\Phi} \tag{14}$$

$$\nabla^2 H_z + \frac{1}{c_S^2}B_z^* = \frac{1}{c_S^2}\ddot{H}_z \tag{15}$$

Assume that

$$\frac{1}{c_P^2}A^* = A \tag{16}$$

$$\frac{1}{c_S^2}B_z^* = B_z \tag{17}$$

Where, A and B_z are the modified pressure excitation potential and shear excitation potential respectively. Equation (16) and (17) become

$$\nabla^2\Phi + \frac{1}{c_P^2}A^* = \frac{1}{c_P^2}\ddot{\Phi} \tag{18}$$

$$\nabla^2 H_z + \frac{1}{c_S^2}B_z^* = \frac{1}{c_S^2}\ddot{H}_z \tag{19}$$

The in-plane strain solution of Equations (18) and (19) can be written using similar formulation presented in ref [22]

$$\bar{\varepsilon}_x = \left(P_S \frac{N_S}{D_S} + P_A \frac{N_A}{D_A} \right) \tag{20}$$

$$\begin{aligned} N_s &= -\xi^2(\xi^2 - \eta_s^2)\cos\eta_p d \sin\eta_s d + 2i\xi^2\eta_p\eta_s \sin\eta_p d \cos\eta_s d \\ N_A &= -\xi^2(2\xi\eta_s\eta_p \sin\eta_s d \sin\eta_p d) - i\xi\eta_s(\xi^2 - \eta_s^2)\sin\eta_p d \sin\eta_s d \end{aligned} \tag{21}$$

$$P_S = (\xi^2 - \eta_s^2)\frac{Ae^{-i\eta_p y_0}}{2\eta_p}\sin\eta_p d_1 + 2\xi\eta_s \frac{B_z e^{-i\eta_s y_0}}{2\eta_s}\cos\eta_s d_1 \tag{22}$$

$$P_A = 2\xi\eta_p \frac{Ae^{-i\eta_p y_0}}{2\eta_p}\cos\eta_p d_1 + (\xi^2 - \eta_s^2)\frac{B_z e^{-i\eta_s y_0}}{2\eta_s}\sin\eta_s d_1 \tag{23}$$

Here P_S and P_A are the source terms for symmetric and antisymmetric Lamb wave modes respectively.

The complete solution of displacement is the superposition of the symmetric, antisymmetric solution (bulk wave solution is not considered here). Displacement solution in the physical domain is obtained by taking inverse Fourier transform of Equation (20)

$$\varepsilon_x = i\left(\sum_{j=0}^{j_s} \left[P_S(\xi_j^S)\frac{N_S(\xi_j^S)}{D_s'(\xi_j^S)} \right] e^{i(\xi_j^S x - \omega t)} + \sum_{j=0}^{j_A} \left[P_A(\xi_j^A)\frac{N_A(\xi_j^A)}{D_A'(\xi_j^A)} \right] e^{i(\xi_j^A x - \omega t)} \right) \tag{24}$$

As we can see from equations (22) and (23), for top surface source ($d_1 = 0$) the sources are decoupled. Therefore, the pressure excitation potential only contributes the A0 Lamb wave mode and shear excitation potentials contributes to only shear excitation potentials.

3. EXPERIMENTAL METHODS

An in situ AE measurement experiment was performed in a steel specimen during a fatigue crack growth experiment. Steel 304 specimen, a commonly used material for nuclear applications was chosen for manufacturing the test specimens. From a large Steel-304 plate, coupons of dimensions 103 mm width, 305 mm length and 1 mm thickness were manufactured by using a vertical metal cutting band saw. The dimensions of the specimen is larger than the conventional MTS fatigue specimen, which are narrower than the present dimension. The wider geometry of the specimen will cause the acoustic waves generating from the crack to travel more distance to the edges. This will cause the signals to die out after reflection from the boundaries due to geometric spreading and material damping before reaching the sensors. The material properties of the specimen material were 200 GPa modulus of elasticity, 8000 kg/m^{3}density, and 0.29 Poisson's ratio.

The experiment for capturing AE due to fatigue crack growth was performed in two stages. In stage 1 a fatigue crack in the specimen was generated by fatigue cyclic loading. The first step in stage one was drilling a circular hole at the geometric center of the specimen. Circular hole at the geometric center of the specimen would cause stress intensity at the edges of the hole during the fatigue loading. This stress intensity would cause generation of fatigue crack at the edges of the hole during fatigue loading. The specimen was mounted on the hydraulic MTS machine and the MTS grips were used to hold the specimen tightly. For the pre crack generation fatigue loading from 30 kN to 3.3 kN at a frequency of 4 Hz was applied. This fatigue loading was applied on the specimen until a tip to tip crack of 6 mm was generated.

Figure 2. Specimen mounted on the MTS machine for fatigue pre-crack generation

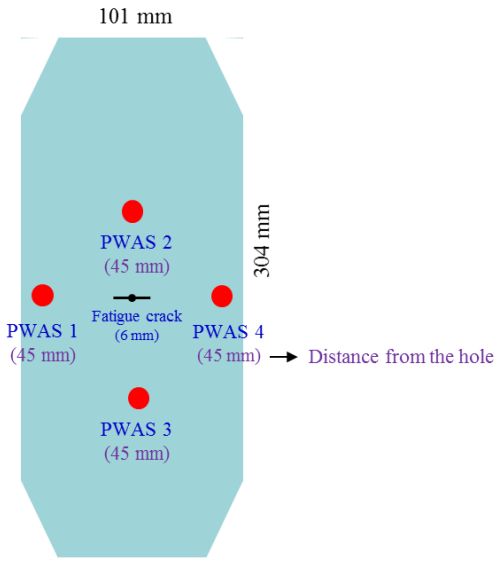

Figure 3. Specimen used for AE signal measurement. Specimen was manufactured of steel 304 material, 103 mm width and 305 mm length

After the generation of the pre-crack (Figure 2), stage 2 of the experiment was performed. During this stage the sensor installation and AE signal capture during the fatigue experiment using the sensors and AE system were performed. After the crack was generated the specimen was taken out of MTS machine and the PWAS sensors were installed on the specimen by using M-Bond 200 adhesive. The sensors were installed in a diamond configuration as represented in Figure 3. This diamond configuration was chosen to observe the angular variation of the AE signals, and to understand in which direction the AE signals are propagating the strongest. The fatigue loading was varied between 18 kN and 1.8 kN (corresponding to 80 % and 8 % of the yield strength of the material) with a loading rate of 0.5 Hz. The AE signals sensed by PWAS were recorded using Mistras AE system. AE signals recorded were post-processed and analyzed.

The experimental set up for capturing AE signal from a fatigue crack growth event is presented in Figure 4. AE signals during crack growth event was captured by four PWAS network installed at a distance 40 mm from the hole as shown in Figure 3. Test specimen installed with PWAS transducer is mounted on MTS machine. The PWAS transducer was connected to acoustic pre- amplifier. The acoustic preamplifier is a band pass filter which filter out signals between 30 to 700 kHz. The pre-amplifier is then connected to 4 channel Mistras AE system for processing the signals.

Test specimen mounted on MTS machine | **Acoustic pre-amplifier** | **Mistras AE instrument**

Figure 4. Experimental set up for capturing fatigue AE signals

4. RESULTS AND DISCUSSION

Figure 5 shows the four different AE signals from PWAS 4 during fatigue crack growth. It can be observed from the figure that the time of flight of the signals is around 17 µs.

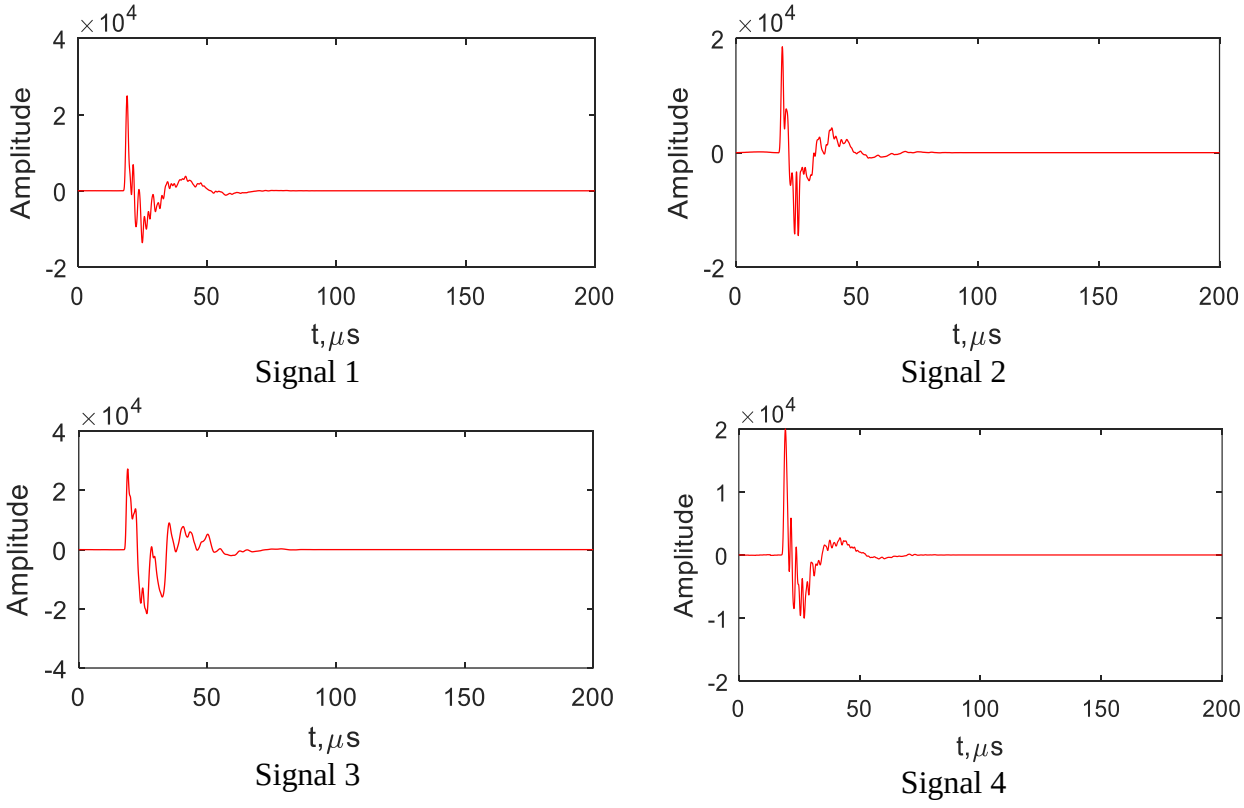

Figure 5. Four different AE signals collected at PWAS 4 during the fatigue crack growth experiment (amplitude is in mV)

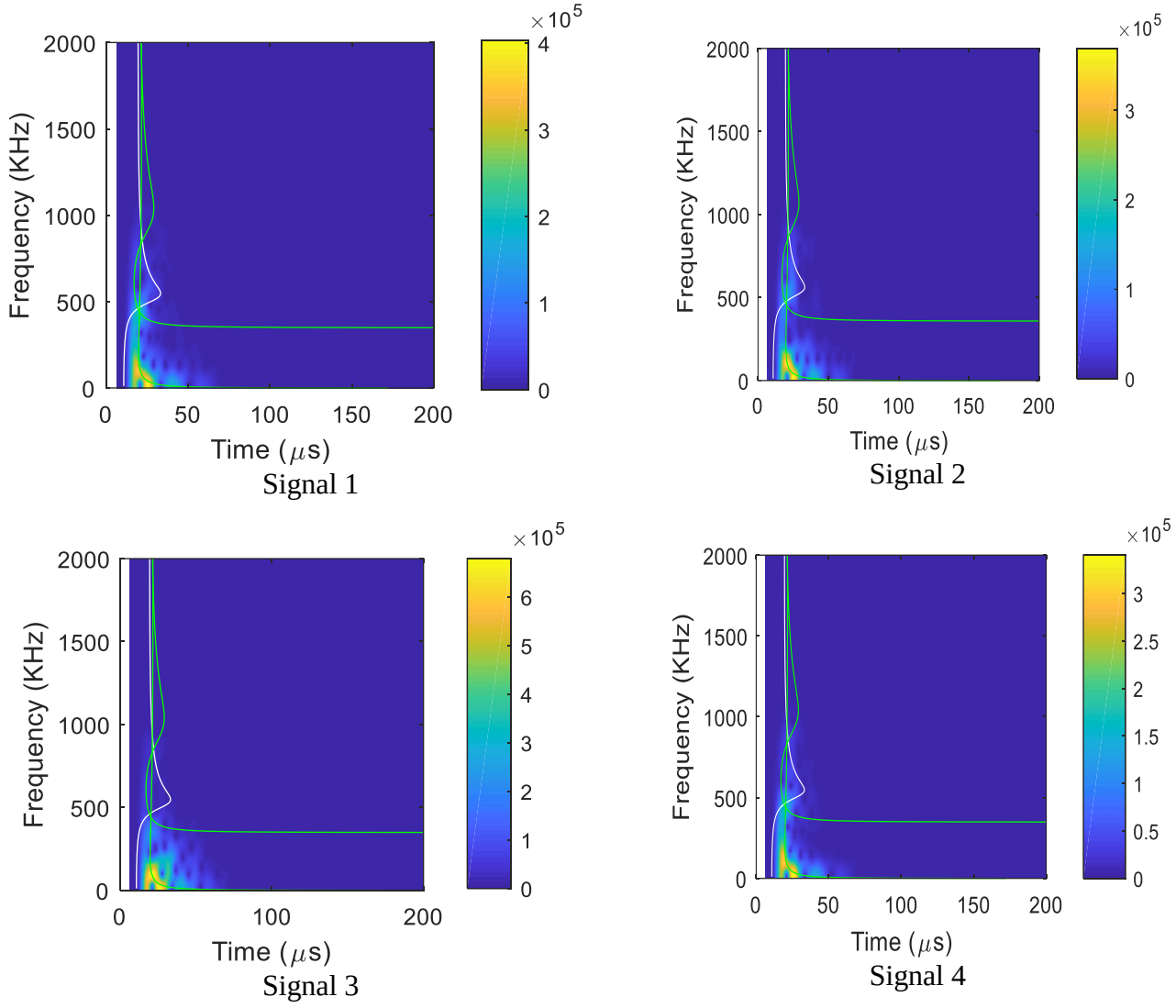

Figure 6. STFT of four AE signals captured. STFT is super-imposed with the time-frequency curves of S0, A0 and SH0 modes.

The qualitative change in the signal can be observed due to the change in the frequency contents. Figure 6 shows the time-frequency analysis of these signals. The short time Fourier transform (STFT) signal is super-imposed with the time-frequency curves of S0, A0 and SH0 modes. This superimposition can identify which wave packet correspond to which Lamb wave mode. It can be illustrated from the figures that there is a slight difference in the frequency contents of the signal. The major frequency contents are in between 30 kHz to 300 kHz. As it can be observed from Figure 6 that the dominant mode is the A0 Lamb wave mode for all of the AE signals. According to equations (22) and (23), top surface source $(d_1 = 0)$ decoupled the Lamb wave modes due to excitation potentials. The pressure excitation potential only contributes the A0 Lamb wave mode and shear excitation potentials contributes to only shear excitation potentials. For 1 mm thick plate the AE source can be assumed as a top surface source. As the AE signal mainly contains A0 mode therefore, the A0 mode should be generated due to pressure potential excitation. An inverse algorithm can be used to find the pressure potential source from the A0 components of the AE guided wave signal from the crack. Figure 7 shows

the inverse algorithm to solve source potential from the received AE signals. In numerical analysis STFT was done on the time domain AE signals to get the separated Lamb wave modes. Then, frequency contents of the AE signal are divided by plate transfer function to get the source term. Then the excitation signals are calculated in frequency domain. Finally, an inverse Fourier transform was done to get the time domain excitation signals from frequency response excitation signals.

Figure 8 shows the de-convoluted time domain excitation signal. As we can see from the figure the time of rise of the four signals are 4.25 µs, 4.63 µs, 4.87 µs and 4.26 µs respectively. The values are very close to each other and confirm that the sources are from the fatigue crack growth. The short rise time of the excitation source refer to a wide band of frequency components.

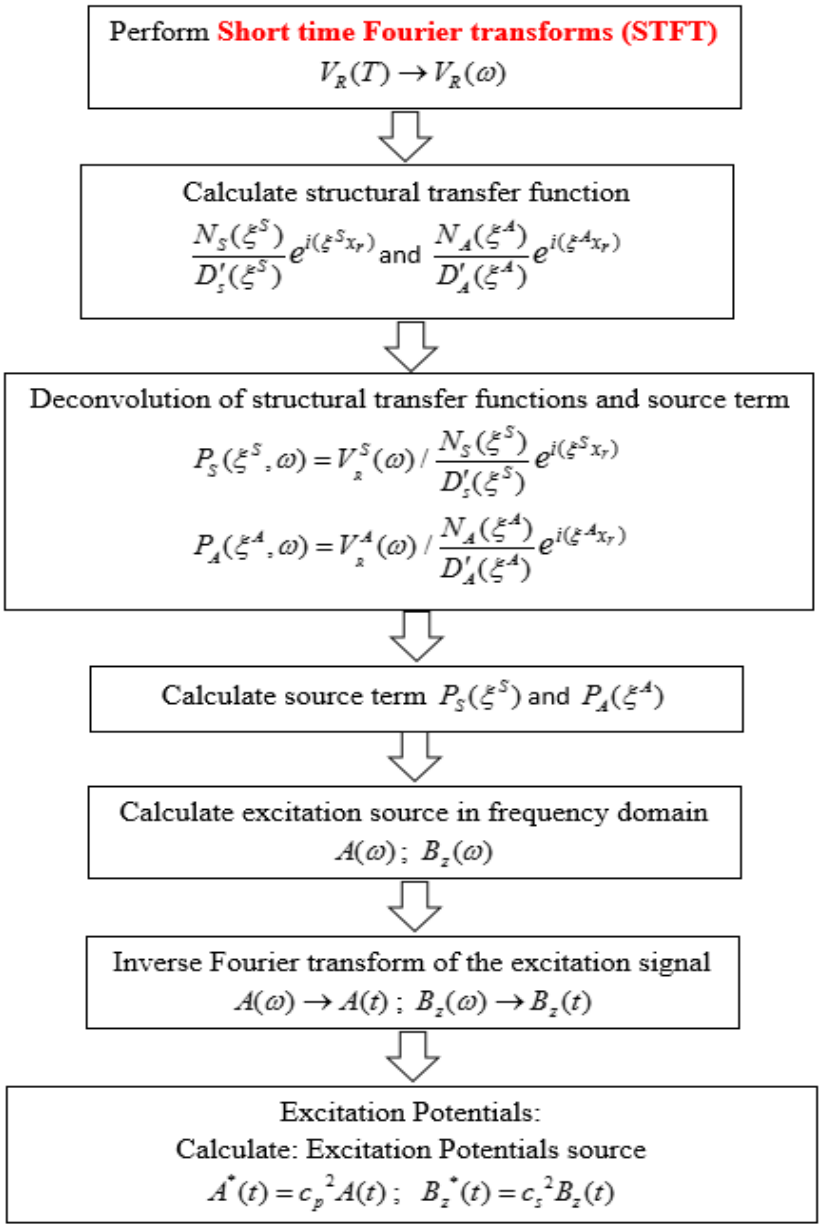

Figure 7. Step by step procedure based on analytical formulations to reconstruct the Helmholtz AE source corresponding to the AE signal

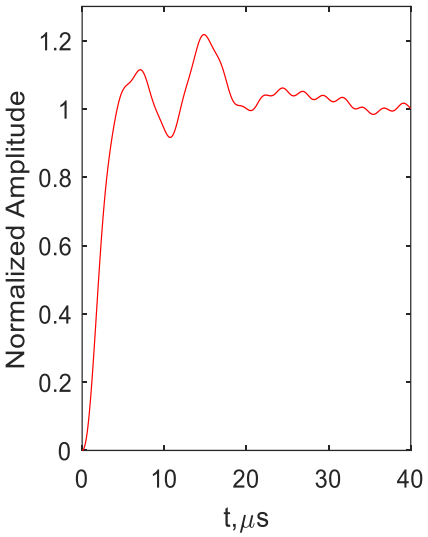

Signal 1
Rise time: 4.25 μs

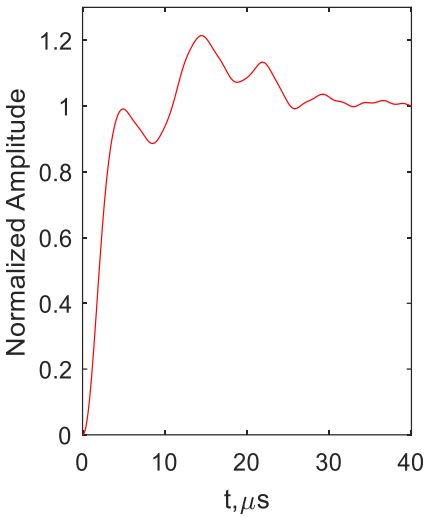

Signal 2
Rise time: 4.63 μs

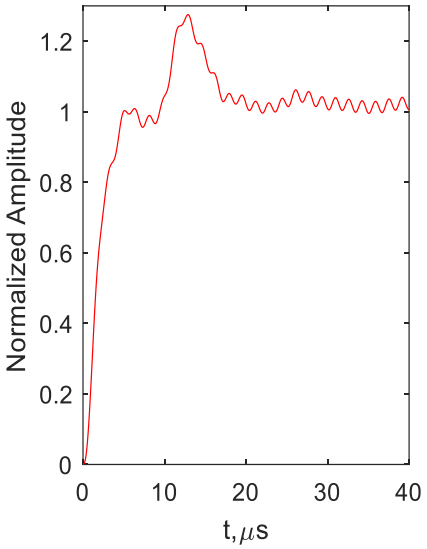

Signal 3
Rise time: 4.87 μs

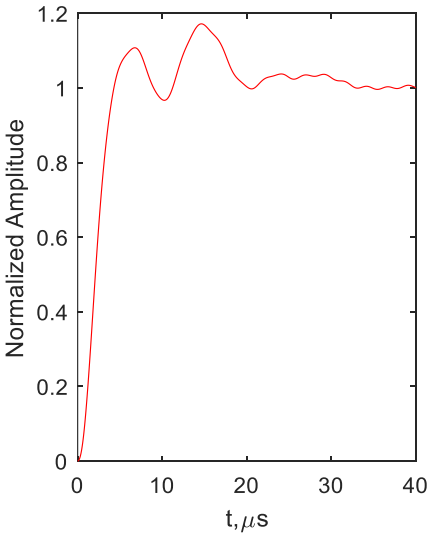

Signal 4
Rise time: 4.26 μs

Figure 8. Helmholtz AE source definition corresponding to the AE signals recorded from fatigue experiment

5. SUMMARY, CONCLUSIONS AND FUTURE WORK

5.1 Summary and conclusions

AE source potentials produce the guided wave in the plate. An experiment was designed to extract physical AE signals from a fatigue crack growth. A time-frequency analysis of time domain signal was done to analyze the frequency content and to separate the Lamb wave modes of the captured AE signals. Frequency contents helped to distinguish different source types. An inverse algorithm was then be developed to characterize the AE source during crack propagation. The rise time was found to be equal for all of the AE signals. Therefore, it can conclude that the AE source are generated from a common source which is a crack tip during crack propagation. The source characterization can provide information about excitation potential released from the crack. Therefore, it may help to generate a qualitative as well quantitative description of the crack propagation phenomenon. This research could help to develop numerical methodology for processing factual data about the amplitude and time-evolution of the AE source potentials. A further extensive study on the effect of plate thickness, AE rise time, and AE source depth would be recommended.

5.2 Future work

A further experimental study on the effect of plate thickness, and AE source depth would be recommended. A correlation between AE source rise time and crack growth rate need to be established.

ACKNOWLEDGEMENT

This work was supported by US Department of Energy (DOE), Office of Nuclear Energy grant numbers DE-NE 0008400, the Air Force Office of Scientific Research (AFOSR) grant number FA9550-16-1-0401, Office of Naval Research (ONR) grant number N00014-17-1-2829, Office of the Vice President for Research, University of South Carolina and crowdfunding from experiment.com.

RFERENCES

[1] M. Y. Bhuiyan and V. Giurgiutiu, “The signatures of acoustic emission waveforms from fatigue crack advancing in thin metallic plates,” *Smart Mater. Struct.*, vol. 27, no. 1, p. 15019, 2018.

[2] H. Mei, M. Haider, R. Joseph, A. Migot, and V. Giurgiutiu, “Recent Advances in Piezoelectric Wafer Active Sensors for Structural Health Monitoring Applications,” *Sensors*, vol. 19, no. 2, p. 383, 2019.

[3] Q. Wang and F. Chu, “Experimental determination of the rubbing location by means of acoustic emission and wavelet transform,” *J. Sound Vib.*, vol. 248, no. 1, pp. 91–103, Nov. 2001.

[4] M. Bentahar and R. El Guerjouma, “Monitoring progressive damage in polymer-based composite using nonlinear dynamics and acoustic emission,” *J. Acoust. Soc. Am.*, vol. 125, no. 1, pp. EL39-EL44, 2009.

[5] M. G. R. Sause, A. Gribov, A. R. Unwin, and S. Horn, “Pattern recognition approach to identify natural clusters of acoustic emission signals,” *Pattern Recognit. Lett.*, vol. 33, no. 1, pp. 17–23, Jan. 2012.

[6] S. M. Cousland and C. M. Scala, “Acoustic emission during the plastic deformation of aluminium alloys 2024 and 2124,” *Mater. Sci. Eng.*, vol. 57, no. 1, pp. 23–29, Jan. 1983.

[7] S. L. McBride, J. W. MacLachlan, and B. P. Paradis, “Acoustic emission and inclusion fracture in 7075 aluminum alloys,” *J. Nondestruct. Eval.*, vol. 2, no. 1, pp. 35–41, 1981.

[8] C. Barile, C. Casavola, and G. Pappalettera, “Acoustic emission waveform analysis in CFRP under Mode I test,” *Eng. Fract. Mech.*, no. December 2017, pp. 0–1, 2018.

[9] S. B. M. Saadatzi, F. Mir, M. N. Saadatzi, V. Tavaf, “Modeling of a 3D acoustoelastic metamaterial energy harvester,” in *Active and Passive Smart Structures and Integrated Systems XII*, 2018.

[10] S. B. M. Saadatzi, F. Mir, M. N. Saadatzi, “Modeling and Fabrication of a Multi-axial Piezoelectric Energy Harvester based on a Metamaterial-inspired Structure,” *IEEE Sens. J.*, vol. 18, no. 22, 2018.

[11] S. B. M. Saadatzi, M. N. Saadatzi, R. Ahmed, “An electro-dynamic 3-dimensional vibration test bed for engineering testing,” in *Industrial and Commercial Applications of Smart Structures Technologies*, 2017.

[12] R. Joseph, M. Y. Bhuiyan, and V. Giurgiutiu, “Acoustic emission source modeling in a plate using buried moment tensors,” *Proc. SPIE (Health Monit. Struct. Biol. Syst.*, vol. 10170, no. May, pp. 1017028-1–8, 2017.

[13] R. Joseph *et al.*, “Active health monitoring of TN32 dry cask using a scaled down model,” *Proc. SPIE (Health Monit. Struct. Biol. Syst*, no. March, 2018.

[14] M. G. R. Sause and S. Horn, “Simulation of Acoustic Emission in Planar Carbon Fiber Reinforced Plastic Specimens,” *J. Nondestruct. Eval.*, vol. 29, no. 2, pp. 123–142, 2010.
[15] M. Åberg, “Numerical modeling of acoustic emission in laminated tensile test specimens,” *Int. J. Solids Struct.*, vol. 38, pp. 6643–6663, 2001.
[16] G. J. Prosser WH, Hamstad MA, “Finite Element and Plate Theory Modeling of Acoustic Emission Waveforms,” *J Nondestruct Eval*, vol. 18, pp. 83–90, 1999.
[17] A. Zelenyak, M. Hamstad, and M. Sause, “Modeling of Acoustic Emission Signal Propagation in Waveguides,” *Sensors*, vol. 15, no. 5, pp. 11805–11822, 2015.
[18] M. A. Hamstad, A. O’Gallagher, and J. Gary, “Modeling of buried monopole and dipole sources of acoustic emission with a finite element technique,” *J. Acoust. Emiss.*, vol. 17, no. 3/4, pp. 97–110, 1999.
[19] J. R. Rice, “Elastic wave emission from damage process,” *J. Nondestruct. Eval.*, vol. 1, no. 4, pp. 215–224, 1980.
[20] P. G. Keiiti A, *Quantitative Seismology*. University Science Books, 2002.
[21] Haider, M. F., Giurgiutiu, V., Lin, B. and Yu, “Simulation of Lamb Wave Propagation using Excitation Potentials,” in *ASME 2017 Pressure Vessels & Piping Conference*, 2017.
[22] Haider, M. F., & Giurgiutiu, V. (2018). A Helmholtz potential approach to the analysis of guided wave generation during acoustic emission events. Journal of Nondestructive Evaluation, Diagnostics and Prognostics of Engineering Systems, 1(2), 021002.
[23] Haider, M. F., & Giurgiutiu, V. (2018). Analysis of axis symmetric circular crested elastic wave generated during crack propagation in a plate: A Helmholtz potential technique. International Journal of Solids and Structures, 134, 130-150.